



Depósito de Investigación
Universidad de Sevilla

Depósito de investigación de la Universidad de Sevilla

<https://idus.us.es/>

“This is an Accepted Manuscript of an article published by Elsevier in Computers and Electronics in Agriculture on March 2012, available at: <https://doi.org/10.1016/j.compag.2012.01.004> .”

21 ABSTRACT

22

23 Digital imaging has become a powerful tool for the characterization and quality
24 control of foodstuff. Because of the need to automate processes, faster tools
25 are needed and Computer Vision is a good alternative to chemical analysis of
26 many products in quality control. Appearance of grape seeds and grape berries
27 change during the ripeness. These changes are closely related to the chemical
28 composition, especially phenolics, which are very important compounds due to
29 their implications on the intensity and stability of red wine colour. In this study, a
30 complete characterization of grape seeds and grape berries by digital image
31 analysis is described. The size of grapes and the veraison has been determined
32 by image analysis and it has been also established an objective browning index
33 of seeds. Morphological differences between varieties were studied by applying
34 discriminant analysis models which allowed us to classify the grape seeds with
35 high accuracy.

36

37 KEYWORDS

38 colour; grape seeds; image analysis; ripeness; *Vitis vinifera*.

39

40 1. INTRODUCTION

41

42 1.1. Colorimetry and food stuff.

43 Colour and appearance are closely related to sensory properties and chemical
44 composition of food. Normally, colour is measured by tristimulus colorimetry.

45 The colour stimulus is composed of three different sensations, giving to colour
46 three-dimensional nature. These attributes are:

47 - Lightness: This feature makes a colour lighter or darker. It is a relative
48 measure of the reflected light against the absorbed. Value 0 is assigned to
49 black and value 100 is assigned to white.

50 - Chroma: It determines for each hue, the colour difference from the grey having
51 the same lightness. It can take positive values from zero.

52 - Hue: It is the main attribute. It is a qualitative property which allows classifying
53 colours as red, yellow, etc. It is related to differences in absorbance of radiant
54 energy at different wavelengths. Hue is specified as an angle.

55 These attributes are often expressed as L^* , C^*_{ab} and h_{ab} , respectively,
56 according to the CIELAB colour space.

57 It can be used different kinds of instruments, such as colorimeters,
58 spectrophotometers and spectroradiometers. Nevertheless, these instruments
59 require homogenizing the sample to achieve uniform colour, which becomes
60 tedious and complicated task to measure colour of heterogeneous stuff or small
61 objects, such as grape berries and grape seeds. In these cases, it is very
62 advantageous the use of digital images for this purpose. Digital image analysis
63 appears as successful complement since it can be determined not only colour

64 but also other characteristics such as shape, texture and homogeneity
65 (Savakar, Dayanand G. et al., 2009; Zheng and Sun, 2008b).

66

67 1.2. Imaging hardware and colour spaces

68 Computer Vision is a subfield of Artificial Intelligence. The aim of Computer
69 Vision is 'teach' a computer for understanding a scene or the characteristics of
70 an image. In this way, we can identify the seeds and grapes in these images,
71 and then, morphological and colorimetric characteristics can be extracted from
72 each one. Computer vision is a powerful tool for testing quality in alimentary
73 industry (Brosnan and Sun, 2004).

74 A computer vision system includes: an illumination system, a charge-coupled
75 device (CCD), a frame grabber which converts the analogue image from the
76 camera into a digitized one, and a computer with the suitable software for image
77 processing and interpretation of results (Wang and Sun, 2002). Illumination
78 system has high importance, not only because of the need to identify objects in
79 the image, but because the colour calculation process needs a light
80 standardization (CIE, 2007). Once the illumination is controlled, a digital camera
81 receives images onto a CCD. It has capacitors which are stimulated by visible
82 radiation and it is registered in gradations of three basic colours: red, green and
83 blue (RGB). This is consistent with the theory that every colour can be
84 reproduced by the combination of three primary colours.

85 The RGB colour space is an additive colour model that uses transmitted light to
86 display colours. It is used for television and other devices screens, so this
87 model is device-dependent (its appearance depends on the display) (Yam and
88 Papadakis, 2004). The L*a*b* model is an international standard for colour

89 measurement developed by the *Commission Internationale d'Eclairage* (CIE) in
90 1976. Here, L^* has the same meaning that the L^* described previously. a^* (from
91 green to red) and b^* (from blue to yellow) are Cartesian coordinates of Polar
92 coordinates C^*_{ab} and h_{ab} previously described. This colour space is device-
93 independent, providing consistent colour regardless of the input or output
94 device such as digital camera, scanner, monitor and printer. CIELAB values are
95 frequently used in food research (González-Miret, Ji et al., 2007).

96 Due to RGB colour space is not continuous each channel can take only integer
97 values between 0 and 255. In order to calculate the colorimetric coordinated
98 recommended by *Comission Internacionale de l'Eclairage* (CIE.), it is necessary
99 to transform from RGB to CIELAB colour spaces. This transformation requires
100 calibration and it depends on illumination when images are taken (León, Mery et
101 al., 2006).

102 One of the most important steps in image analysis is segmentation.
103 Segmentation refers to the process of partitioning a digital image into multiple
104 segments (sets of pixels). The goal of segmentation is to simplify and/or change
105 the representation of an image into something more meaningful and easier to
106106 analyze (Zheng and Sun, 2008a).

107107

108 1.3. Advantages of using image analysis for grapes and grape seeds
109 characterization.

110 The size of the grapes is measured in routine analysis during ripening. The
111 diameter is normally measured with a calliper, which measures the size in only
112 one direction and the mean of several grapes is given, making this a tedious
113 task. In addition, the berry could be accidentally tightened during measurement

114 and it induces error. For this purpose, the use of Feret diameter has been
115 proposed (González Marcos, Martínez de Pisón Ascacibar et al., 2006). Feret
116 diameter is the maximum length of chord for a counterclockwise angle with the
117 x axis, defined between 0° and 180° (Figure 1). Due to grape berries are not
118 completely spherical, for each berry, the mean of all Feret diameters for all
119 possible angles have been considered. This way, the size will be given as an
120 average of all possible Feret diameters of all the grapes analyzed.

121 During the grapes ripening there is a loss of chlorophyll and the formation of the
122 final dyes. This process starts at the *veraison*, the onset of ripening, when the
123 colour of the grape berries change, being the transition from berry growth to
124 berry ripening. In red grapes, the colour changes from green to purple, even
125 almost black. The *veraison* is normally expressed as a percentage determined
126 by visual inspection. It is possible to establish an objective *veraison* index by
127 image analysis.

128 There are more appearance-related characteristics of the seeds and grapes
129 associated to maturity, such as the browning of the seeds (Ristic and Iland,
130 2005). All these parameters can be estimated of an objective and automated
131 manner by image analysis.

132

133 2. MATERIAL AND METHODS

134 2.1. Sampling.

135 The vineyards sampled are included under the “Condado de Huelva”
136 Designation of Origin, in southwestern Spain, harvested in 2009 and 2010. Two
137 red varieties (*Tempranillo* and *Syrah*) and one autochthonous white variety
138 (*Zalema*) cultivated in two kinds of soil (*Sand* and *Clay*) were used. Samples

139 were taken twice a week from early July until harvest (which occurred
140 approximately at end of August depending on variety). Sampling was carried
141 out taking a pair of berries from alternate grapevines and from both sides up to
142 reach 2 Kg of berries, ensuring this way the representativeness of the sample.
143 Once in lab, one hundred berries were randomly taken and cleaned for
144 acquiring the images. Seeds of these berries were removed and dried at room
145145 temperature for two hours before acquiring the image.

146146

147 2.2. Apparatus

148 The DigiEye® imaging system based upon the calibrated digital camera was
149 used (Luo, Cui et al., 2001). It includes an illumination box specially designed
150 by VeriVide Ltd. (Leicester, UK) to illuminate the samples consistently and a
151 digital camera connected to a computer (Figure 2).

152 The digital camera used for image acquisition was 10.2-megapixel Nikon® D80
153 with Nikkor® 35 mm f/2D objective. The camera was connected via USB to a
154 computer with Pentium IV processor at 3.00 GHz. The cabinet is equipped with
155 two fluorescent tubes that emulate the standard illuminant D65 and offer stable
156 lighting conditions. Lamps were switched on at least ten minutes before being
157 used, according to manufacturer indications, to stabilize them.

158 For obtaining morphological and appearance parameters, as well as CIELAB
159 coordinates from RGB colour space, the software DigiFood® (Heredia,
160160 Gonzalez-Miret et al., 2006) was used.

161161

162 3. RESULTS

163 3.1. Image acquisition

164 The camera parameters were set up for all images as shown in Table 1. To
165 ensure that the camera always takes images the same way, calibration is
166 required prior to use by a certified colour chart DigiTizer provided by VeriVide
167 Ltd. (Leicester, UK) (Figure 3), composed of a matrix of 12 × 20 squares of
168 different colours. DigiEye have data of the L*a*b* coordinates of each square
169 and adapt the RGB coordinates obtained by the camera for this calibration.
170 Several backgrounds were tested for image acquisition of grapes and seeds.
171 Among them, it was found that the white surface increases the contrast
172 between objects and background, and improves the segmentation process.
173 Once the background was selected, both seeds and berries were put avoiding
174 contact among them over a white thick sheet, considered as a good Lambertian
175 surface (diffuse reflectance surface which does not vary depending on the
176 viewing angle) (Jaglariz, Duraj et al., 2006).

177

178 3.2. Image processing

179 Although the analytical information was obtained from the CIELAB coordinates
180 calculated, HSI (hue, saturation and intensity) colour space was used for
181 segmentation process (Jack, 2008). HSI colour space is easier to understand
182 than RGB, due to its likeness with the L*, C*_{ab} and h_{ab} stimuli.

183 The histogram thresholding segmentation technique was used (Cheng, Jiang et
184 al., 2001). It allows distinguish different objects in images that are composed of
185 regions with different colour ranges. Histograms of HIS values were plotted,
186 containing well separated peaks corresponding to the sample and the
187 background. The lowest point between adjacent peaks was stated as threshold

188 for segmentation process. After establishing the thresholds, the suitability of the
189 criteria was confirmed by visual inspection.

190 For grape berries recognition, all regions having intensity (I) between 0 and 160
191 units were considered. Restrictions in hue (H) and saturation (S) values were
192 not required for grapes berries. To prevent the recognition of small spots as
193 grapes, the segmentation was restricted to objects having Feret diameter
194 between 5 and 25 mm.

195 In the same way, for seeds recognition, sets of pixels with saturation (S)
196 between 0 and 180 units and intensity (I) between 0 and 140 units were
197 considered. All hues (H) were considered. Similarly, morphological restrictions
198 were applied. All objects must have area between 6 and 35 mm² and length
199 shorter than 15 mm for being considered (Figure 4).

200 The following morphological and appearance parameters were measured from
201 segmented images of seeds:

202 RGB colour was obtained from the raw images. CIELAB colour coordinates
203 were obtained from the RGB values and through the camera calibration. All
204 images were acquired under the same conditions. Thus, taking a picture of the
205 calliper, it was possible to calculate the conversion between units of length and
206 pixels. The size of seeds was measured in two directions: diameter along major
207 axis of the seed (length) and diameter along the axis perpendicular to the major
208 axis (width). In order to measure the elongation degree of each seed, aspect
209 ratio was calculated, which is ratio is the ratio between major axis and minor
210 axis of the ellipse equivalent to the seed. Roundness values were calculated
211 using the following dimensionless equation (González Marcos, Martínez de
212 Pisón Ascacibar et al., 2006):

213213 Roundness: $\frac{perimeter^2}{4 \times \pi \times area}$

214 In this sense, a perfect circle has a roundness value of 1 and it becomes higher
215 while the shape elongates. Some authors use the inverse of this equation for
216 the same purpose. The area of each pixel was calculated by the spatial
217 calibration. Thus, the area of each seed was calculated by pixel count.

218 Measuring colour of each pixel, it is possible to have an estimation of the
219 heterogeneity of the sample as the fraction of pixels that deviate more than 10%
220 from the average intensity. Other indicator of heterogeneity is obtained by using
221 the Mean Colour Difference from the Mean (MCDM), proposed by Berns (2000):

222222
$$MCDM = \frac{\sum_{i=1}^N \left[(L_i^* - \bar{L}^*)^2 + (a_i^* - \bar{a}^*)^2 + (b_i^* - \bar{b}^*)^2 \right]^{1/2}}{N}.$$

223223

224 3.3. Study of appearance and colorimetric evolution of grapes and grape seeds.

225 3.3.1 Varietal classification by morphology

226 From morphological data of all samples corresponding to the four grapes
227 varieties considered in this study, analysis of variance ANOVA with Statistica®
228 8.0 (StatSoft Inc., 2007) was applied. The aim of considering all samples was to
229 distinguish among varieties regardless the moment of sampling. Significant
230 differences ($p < 0.05$) in the morphology of seeds from different grape varieties
231 were found. No differences regarding the soil type for the white variety were
232 found (Table 2).

233 Discriminant analysis was applied to classify the samples based on the features
234 of appearance of the seed. Based on seeds from red grapes or white grapes,
235 the classification was 100%. The classification between the two red varieties

236 was 100% for Syrah and 87.5% for Tempranillo. When only the white variety
237 was considered, it was not possible to discriminate correctly between soil types
238 by morphological features. The classification for Zalema Sand was 71.43%
239 while for Zalema Clay was only 57.14%. In general, the parameters *aspect*
240240 *ratio*, *roundness* and *width* gain more weight in the equations.

241241

242 3.3.2 Evolution of the appearance of seeds during maturation.

243 According to the variety, similar changes occur in grape seed during the
244 maturation. Colorimetric parameters decrease quickly in the first stages and
245 stabilize themselves in the last ones (Figure 6-a, b & c). However, a related fit is
246 visible in the figure depending on the type of grape (red or white). There was no
247 noteworthy change in the shape of the seeds in this period. Nevertheless, the
248 graph clearly shows the difference between the size of the seeds of red and
249 white varieties (Figure 6-d). These differences were essential in the discriminant
250 analysis described above. The Figure 6-f shows how natural darkening of seeds
251 produces the decrease of the mean CIELAB color difference from the mean
252252 MCDM, being this lastest colour more homogeneous.

253253

254 *Browning index*

255 Colour heterogeneity increases in the early stages of maturation and decreases
256 in the final stages, because browning process does not occur in a
257 homogeneous manner. The seeds become dark brown bit by bit while the light
258 green areas disappear in the same way. Histograms of L* for the initial and final
259 samples were overlaid in order to study the behaviour. Both histograms crossed

260 in the value $L^*=50$ (Figure 5). Thus, "Browning Index" was defined the as
261 fraction of pixel having L^* value lower than 50 CIELAB units.

$$262262 \quad \text{Browning Index} = \frac{\text{No.of pixels with } L^* < 50 \text{ units}}{\text{No. totalpixels}}$$

263 During maturation, the Browning Index increased rapidly at the early stages
264 while it is stabilized at the final stages when the seed was almost completely
265265 dark brown (Figure 6-f).

266266

267 *Colour ellipses*

268 By spectroradiometry, we obtain the average from the measured area. In colour
269 analysis by digitalization, we obtain a measure from each pixel from the image.
270 After processing the images, all colour points corresponding to a sample were
271 plotted in the a^*b^* -diagram. Regarding the evolution of these "clouds of points "
272 it can be appreciated how the chromatic dispersion decreases over time. In the
273 early stages, the seeds are pale green mixed with light brown, which evolve
274 until the harvest, producing a clear convergence towards dark brown colours.
275 These points give information about the chromatic heterogeneity of the sample,
276 and they can be fitted to an ellipse for its quantification. The ellipse is oriented
277 along the line of least squares linear fit of these points. The centre of the ellipse
278 coincides with the mean of a^* and b^* values and its semiaxis are proportional to
279 the dispersion of the points (Figure 7). It was found high correlation ($r^2=0.98$)
280 between the length of the ellipses containing the pixels of one sample and the
281 standard deviation of chroma corresponding to these pixels (C^*_{ab}) (Figure 8).

282282

283 3.3.3. Evolution of the appearance of grapes during maturation.

284 A group of berries were taken and their veraison were assigned by visual
285 assessment. The unripe berries are clearly green. Then, its colour turns lighter
286 and begins to appear pink zones. Finally, the skin colour moves forward purple
287 almost black. For each berry, the veraison is considered complete when the
288 colour reaches this deep purple.

289 A criterion based on the bright was enough to assess the veraison level. After
290 identifying the grape berries within the images, the RGB values of grapes
291 before and after veraison were studied. The following threshold was
292292 established:

$$\begin{aligned} \frac{R+G+B}{3} \geq 90 &\rightarrow \text{pre- veraison} \\ \frac{R+G+B}{3} < 90 &\rightarrow \text{post- veraison} \end{aligned}$$

294 As performed by visual assessment, the veraison was calculated for each
295 sample (group of grapes) as the percentage of berries that meet the threshold
296296 set (Figure 9).

297297

298 4. CONCLUSIONS

299 The appearance of grape seeds has been assessed along two months
300 corresponding to the final stages of ripening in two vintages. Within the same
301 grape variety, the morphology of the seeds does not change during the period
302 considered. However, there are significant differences ($p < 0.05$) among
303 varieties, so we can use these parameters for varietal discrimination. Except for
304 the Zalema cv., which two kinds of samples were considered regarding the type
305 of soil, classification was successful, being the aspect ratio and the roundness
306 the variables that induced the differences.

307 The threshold chosen from the overlap of initial and final histograms of lightness
308 (L^*) was the same for the two vintages considered (2009 and 2010). So, the
309 browning index proposed is a good criterion for estimating the maturity of
310 grapes seeds.

311 The colour ellipses containing most of pixels from an image are measurable,
312 clearly express the average colour and the chromatic heterogeneity of these
313 samples, and there is a clear relationship between the size of the ellipse and
314 the standard deviation of chroma (C^*_{ab}).

315 Veraison and the size of the grape berries are characteristics routinely
316 assessed during maturation. It has been established an effective and objective
317 criteria for the veraison assessment as well as a measure of size faster and
318 more accurate than that obtained manually using a calliper based on digital
319 image analysis.

320 In short, the image analysis is becoming a fast and successful tool for the
321 evaluation of food products. It is possible to use these tools to characterize the
322 colour, morphology and appearance of the grapes and their seeds in a
323323 comprehensive manner.

324324

325 ACKNOWLEDGEMENTS

326 We thank the Ministry of Science and Innovation of Spain (Project AGL2008-
327 05569-C02-02) and the concession of the fellowship (BES-2009-025429) for
328328 financial support.

329329

330 REFERENCES

- 331 Berns, R., 2000. Billmeyer and Saltzman's principles of color technology. Willey,
332 New York.
- 333 Brosnan, T. and Sun, D.W., 2004. Improving quality inspection of food products
334 by computer vision—a review. *Journal of Food Engineering* 61, 3-16.
- 335 Cheng, H.D., Jiang, X.H., Sun, Y., and Wang, J., 2001. Color image
336 segmentation: advances and prospects. *Pattern Recognition* 34, 2259-2281.
- 337 CIE, 2007. Commission internationale de l'Eclairage. Standard Illuminants for
338 Colorimetry. ISO 11664-2:2007.
- 339 González Marcos, A., Martínez de Pisón Ascacibar, F.J., Pernía Espinoza,
340 A.V., Alba Elías, F., Castejón Limas, M., Ordieres Meré, J., and Vergara
341 González, E., 2006. *Técnicas y Algoritmos Básicos de Visión Artificial*.
342 Universidad de La Rioja, Logroño.
- 343 González-Miret, M.L., Ji, W., Luo, R., Hutchings, J., and Heredia, F.J., 2007.
344 Measuring colour appearance of red wines. *Food Quality and Preference* 18,
345 862-871.
- 346 Heredia, F.J., Gonzalez-Miret, M.L., Álvarez, C., and Ramírez, A., 2006
347 DigiFood. Registro N° SE-01298.
- 348 Jack, K., 2008. Color Spaces. In: *Digital Video and DSP*. Newnes, Burlington,
349 pp. 15-29.

350 Jaglariz, J., Duraj, R., Szopa, P., Cisowski, J., and Czernastek, H., 2006.
351 Investigation of white standards by means of bidirectional reflection distribution
352 function and integrating sphere methods. *Optica Applicata* 36, 97-103.

353 León, K., Mery, D., Pedreschi, F., and León, J., 2006. Color measurement in
354 L*a*b* units from RGB digital images. *Food Research International* 39, 1084-
355 1091.

356 Luo, M.R., Cui, G.H., and Li.C, 2001 British Patent (Application No. 0124683.4)
357 entitled Apparatus and method for measuring colour (DigiEye System), Derby
358 University Enterprises Limited.

359 Ristic, R. and Iland, P.G., 2005. Relationships between seed and berry
360 development of *Vitis Vinifera* L. cv Shiraz: Developmental changes in seed
361 morphology and phenolic composition. *Australian Journal of Grape and Wine*
362 *Research* 11, 43-58.

363 Savakar, D.G. and Anami, B.S., 2009. Recognition and Classification of Food
364 Grains, Fruits and Flowers Using Machine Vision. *International Journal of Food*
365 *Engineering* 5, Article 14.

366 StatSoft Inc., 2007 Statistica 8.0. Tulsa, USA

367 Wang, H.H. and Sun, D.W., 2002. Correlation between Cheese Meltability
368 Determined with a Computer Vision Method and with Arnott and Schreiber
369 Tests. *Journal of Food Science* 67, 745-749.

370 Yam, K.L. and Papadakis, S.E., 2004. A simple digital imaging method for
371 measuring and analyzing color of food surfaces. Journal of Food Engineering
372 61, 137-142.

373 Zheng, C. and Sun, D.W., 2008a. Image Segmentation Techniques. In: Da-
374 Wen, S. (Ed.), Computer Vision Technology for Food Quality Evaluation
375 Academic Press, Amsterdam, pp. 37-56.

376 Zheng, C. and Sun, D.W., 2008b. Object Measurement Methods. In: Da-Wen,
377 S. (Ed.), Computer Vision Technology for Food Quality Evaluation Academic
378378 Press, Amsterdam, pp. 57-80.

379379

380 FIGURE CAPTIONS

381a) FIGURE 1: b) Feret diameters at 0° and 90° .

382 FIGURE 2: The DigiEye[®] System: (1) illumination box; (2) digital camera; (3)
383 computer.

384 FIGURE 3: Colour chart used for the calibration of the digital camera.

385 FIGURE 4. Image of Syrah seeds and the resulting mask after segmentation.

386 FIGURE 5. Overlap of the histograms of L^* for the initial and final samples.

387 FIGURE 6: Evolution of the Browning Index of seeds during the ripening.

388 FIGURE 7: Scatterplot of seed colour and ellipse fitting.

389 FIGURE 8: Correlation between Std. Dev. of chroma (C^*_{ab}) and length of
390 ellipse.

391 FIGURE 9: Segmentation mask and veraison assessment by the selected
392 criterion.

TABLE 1: Camera setup.

Time exposure	1/15 s
Aperture	f/6.3
Sensitivity	200 ISO
Format	TIF
Image size	3872x2592
Resolution	96 pixels per inch (ppi)

TABLE 2: Some morphological parameters measured in seeds regarding the variety. (Mean \pm Std.Dev.)

	Syrah	Tempranillo	Zalema (sand)	Zalema (clay)
Length (mm)	6.6 \pm 0.2 ^a	6.8 \pm 0.2 ^a	5.7 \pm 0.1 ^b	5.7 \pm 0.1 ^b
Width (mm)	3.8 \pm 0.1 ^b	4.0 \pm 0.1 ^a	3.6 \pm 0.1 ^c	3.6 \pm 0.1 ^c
Aspect Ratio	1.80 \pm 0.01 ^a	1.72 \pm 0.01 ^b	1.64 \pm 0.01 ^c	1.64 \pm 0.01 ^c
Roundness	1.31 \pm 0.02 ^a	1.26 \pm 0.03 ^b	1.24 \pm 0.03 ^b	1.24 \pm 0.02 ^b
Perimeter (mm)	16.91 \pm 0.08 ^b	17.50 \pm 0.09 ^a	14.85 \pm 0.07 ^c	14.76 \pm 0.07 ^c
Area (mm²)	17.3 \pm 0.7 ^b	19.1 \pm 1.1 ^a	14.1 \pm 0.9 ^c	13.9 \pm 0.7 ^c
Heterogeneity	17.5% \pm 0.6% ^a	13.9% \pm 0.7% ^b	15.4% \pm 0.5% ^{ab}	14.7% \pm 0.5% ^{ab}

Figure 1
[Click here to download Figure: Rodriguez-Pulido_FIGURE1.eps](#)

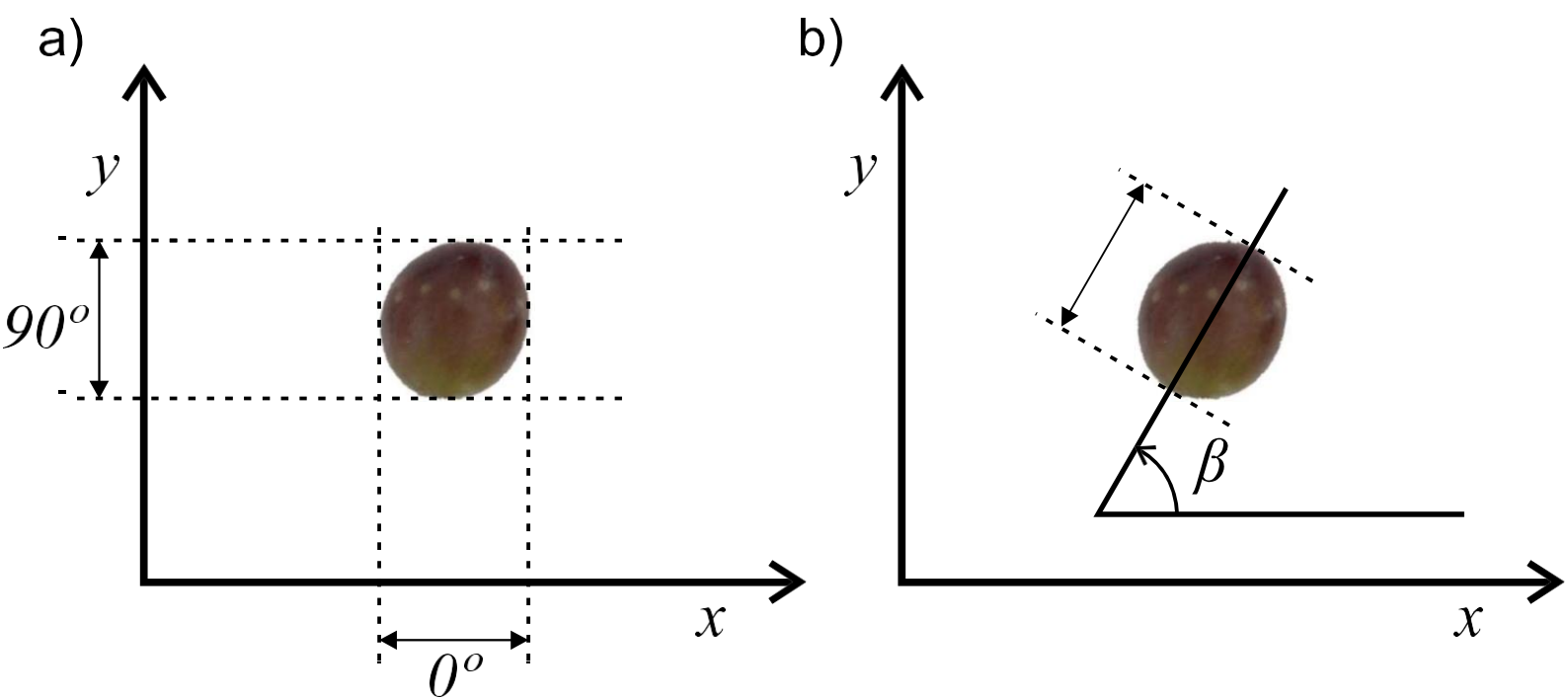


Figure 2
[Click here to download Figure: Rodriguez-Pulido_FIGURE2.eps](#)

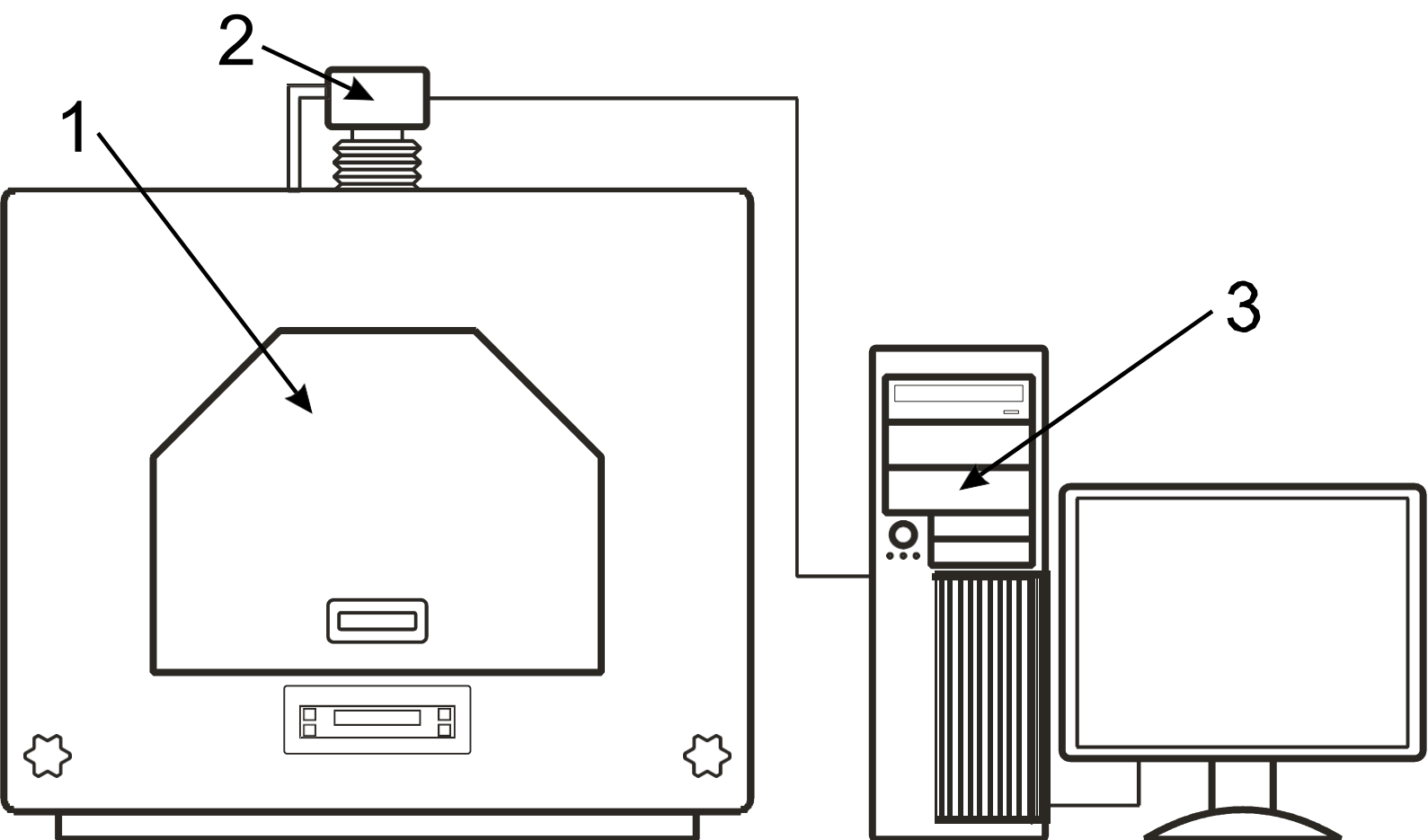


Figure 3

[Click here to download high resolution image](#)



Figure 4

[Click here to download high resolution image](#)

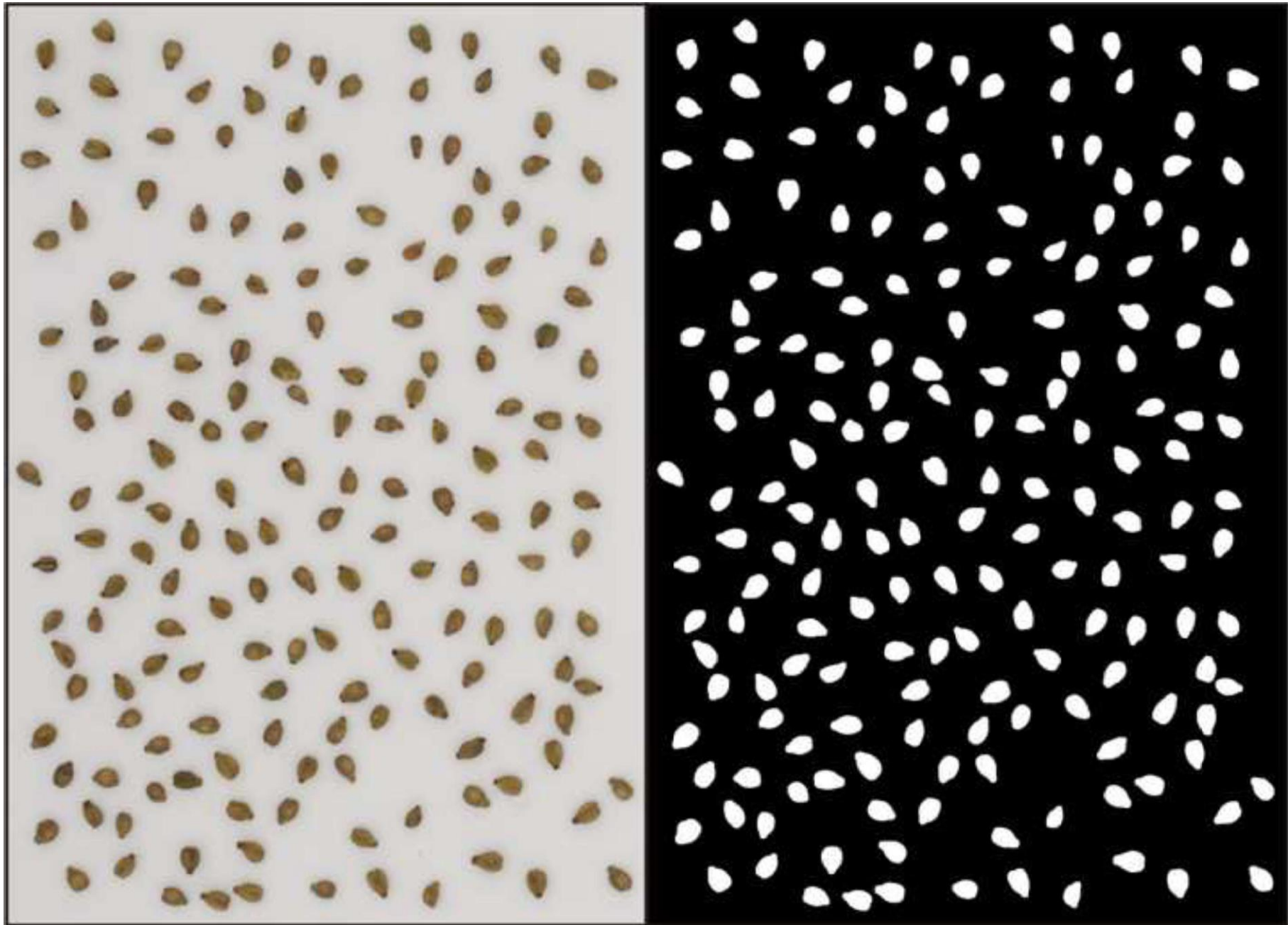


Figure 5
[Click here to download Figure: Rodriguez-Pulido_FIGURE5.eps](#)

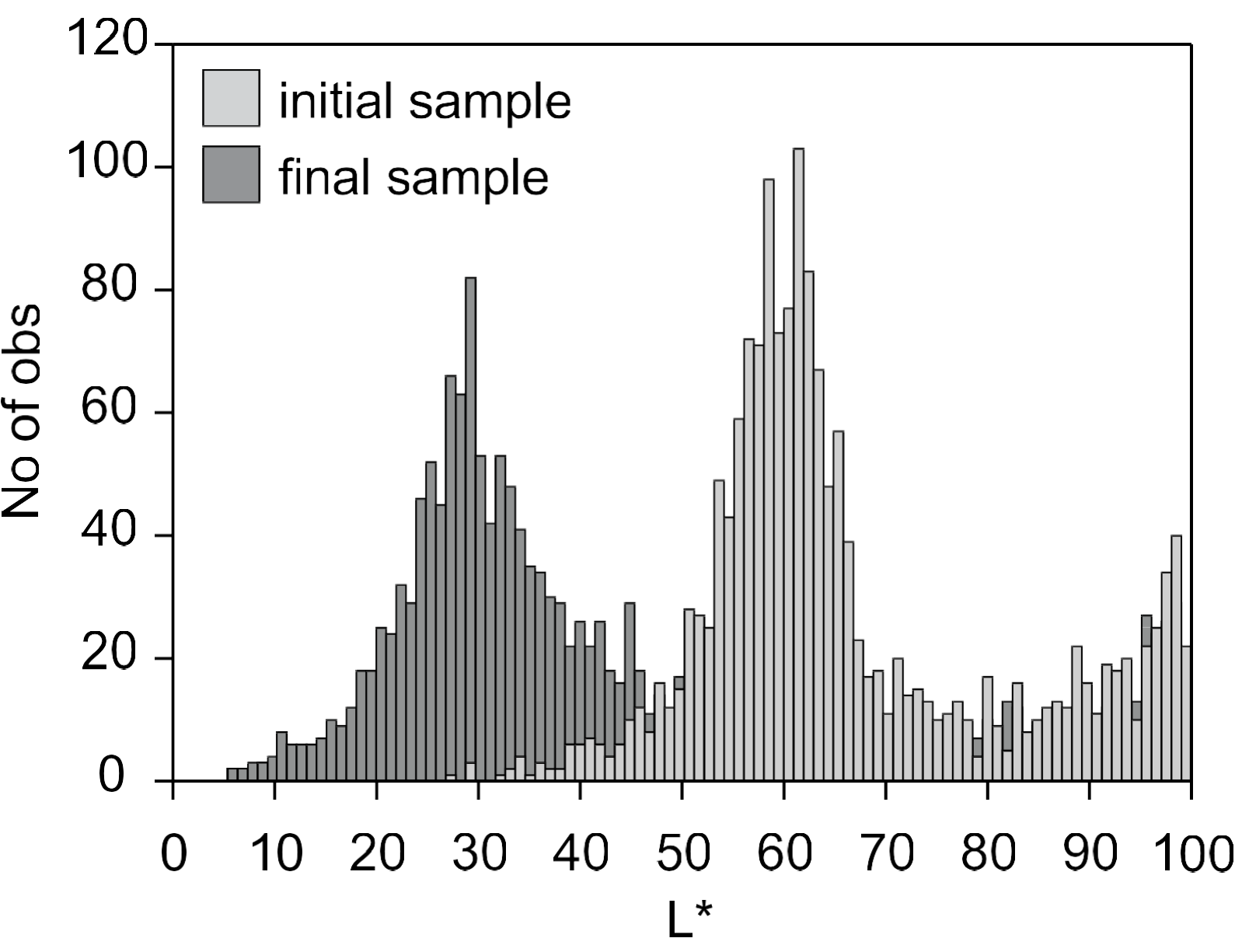


Figure 6
[Click here to download Figure: Rodrguez-Pulido_FIGURE6_rev.eps](#)

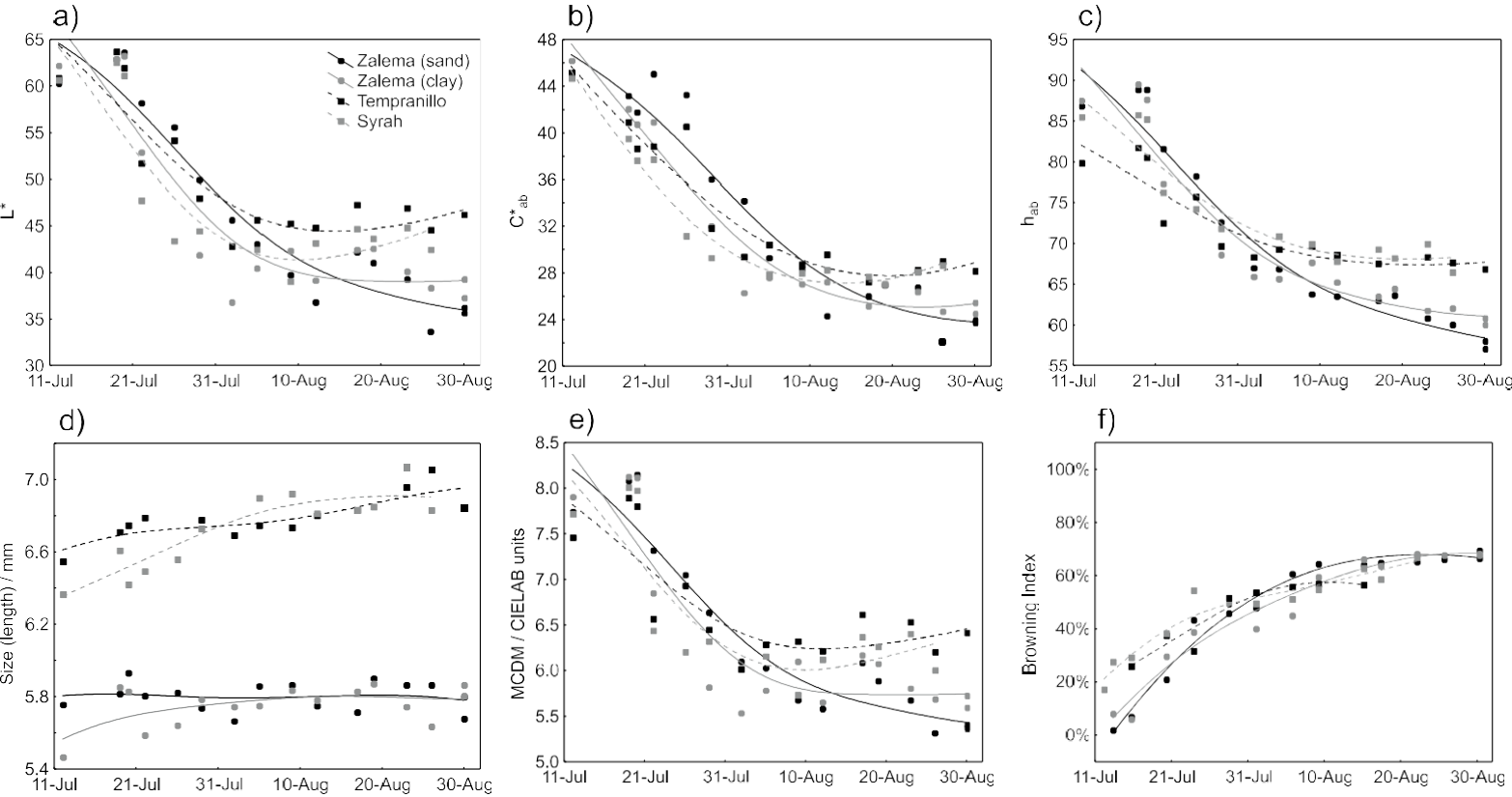


Figure 7
[Click here to download Figure: Rodriguez-Pulido_FIGURE7.eps](#)

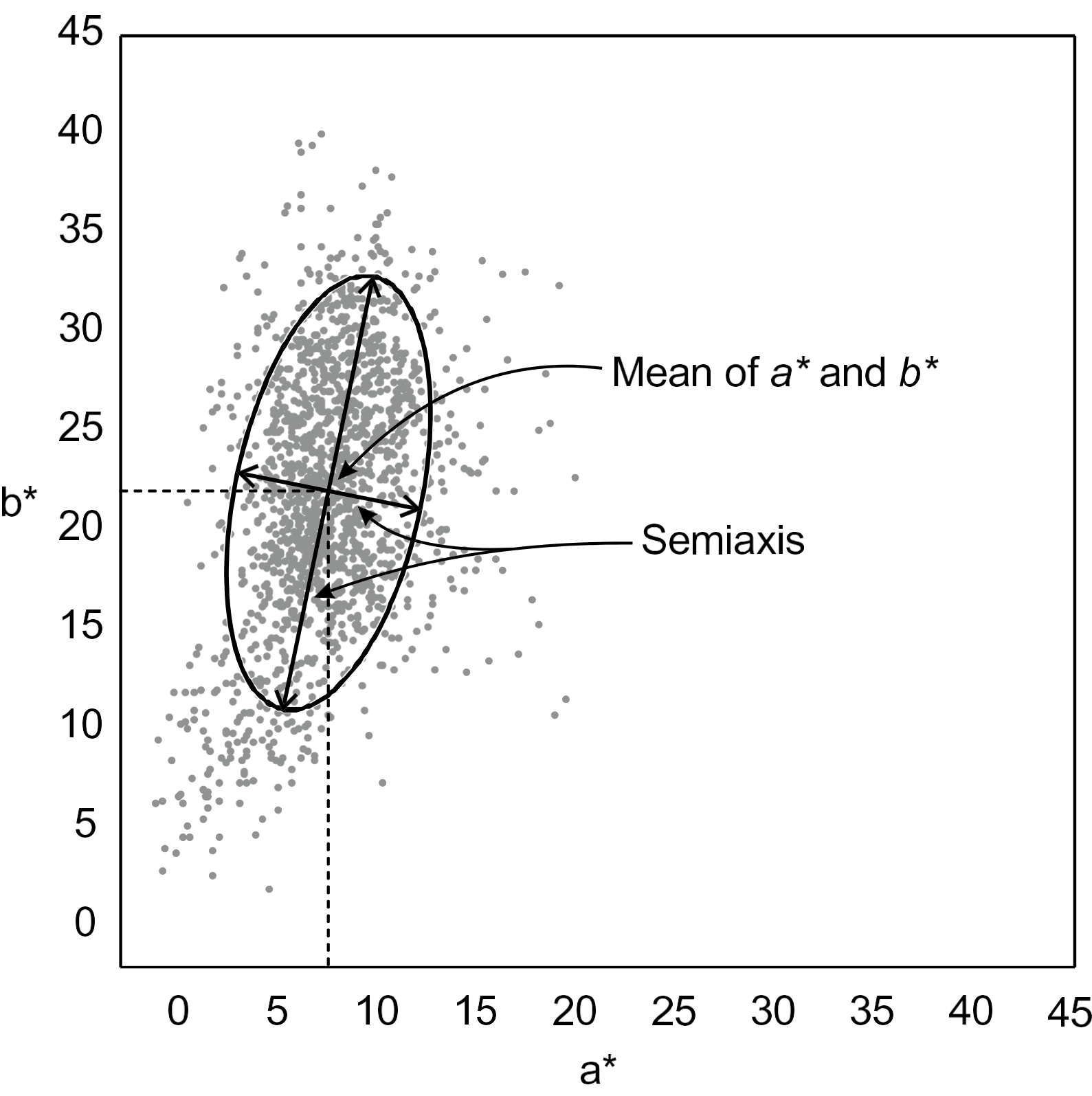


Figure 8
[Click here to download Figure: Rodriguez-Pulido_FIGURE8.eps](#)

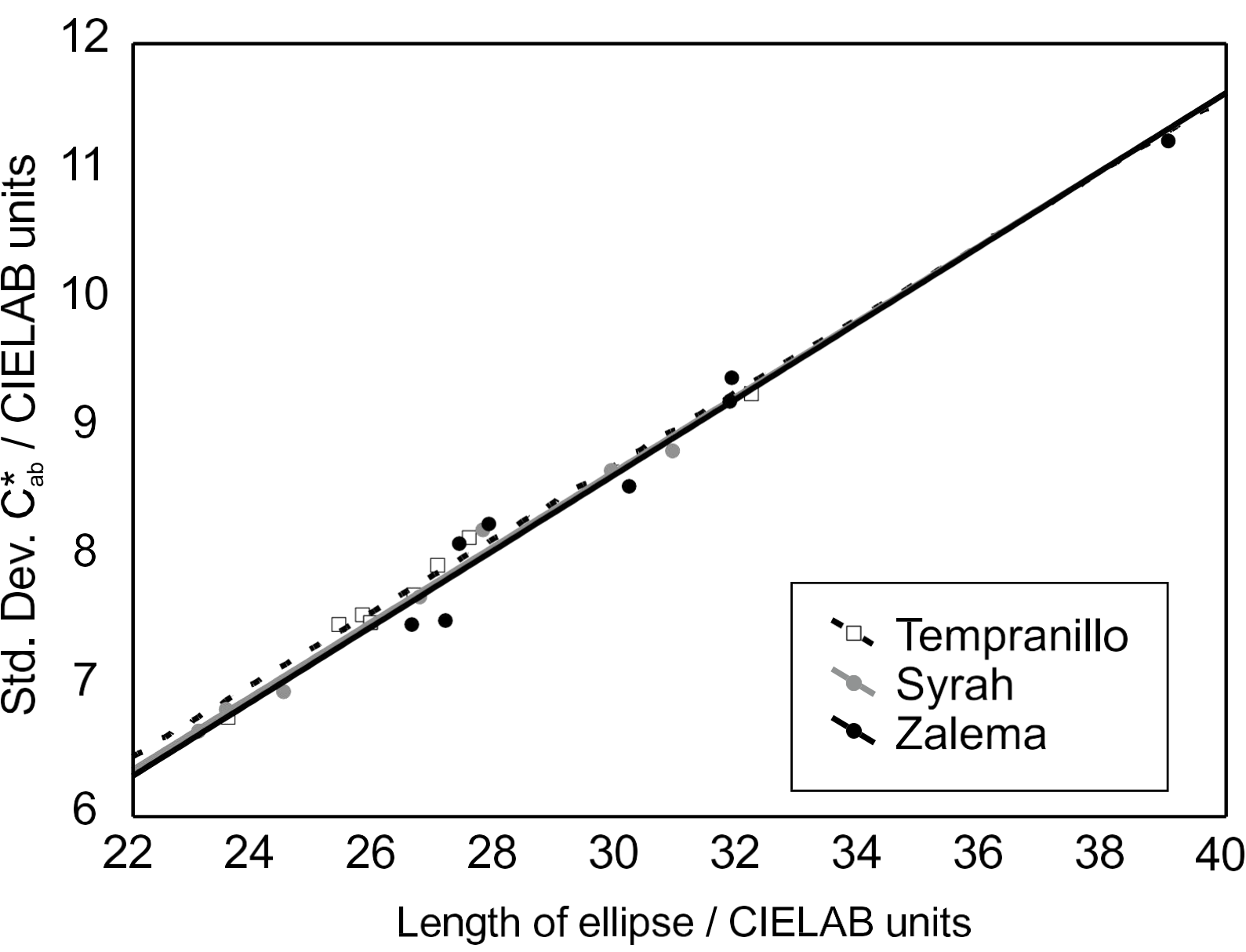


Figure 9

[Click here to download high resolution image](#)

